

Study of the $K_L^0 \rightarrow \pi^0 \pi^0 \nu \bar{\nu}$ decay

R. Ogata,¹ S. Suzuki,¹ J. K. Ahn,² Y. Akune,¹ V. Baranov,³ K. F. Chen,⁴ J. Comfort,⁵ M. Doroshenko,^{6,*} Y. Fujioka,¹ Y. B. Hsiung,⁴ T. Inagaki,^{6,7} S. Ishibashi,¹ N. Ishihara,⁷ H. Ishii,⁸ E. Iwai,⁸ T. Iwata,⁹ I. Kato,⁹ S. Kobayashi,¹ S. Komatsu,⁸ T. K. Komatsubara,⁷ A. S. Kurilin,³ E. Kuzmin,³ A. Lednev,^{10,11} H. S. Lee,² S. Y. Lee,² G. Y. Lim,⁷ J. Ma,¹¹ T. Matsumura,¹² A. Moiseenko,³ H. Morii,^{13,†} T. Morimoto,⁷ Y. Nakajima,¹³ T. Nakano,¹⁴ H. Nanjo,¹³ N. Nishi,⁸ J. Nix,¹¹ T. Nomura,^{13,†} M. Nomachi,⁸ H. Okuno,⁷ K. Omata,⁷ G. N. Perdue,^{11,‡} S. Perov,³ S. Podolsky,^{3,§} S. Porokhovoy,³ K. Sakashita,^{8,†} T. Sasaki,⁹ N. Sasao,¹³ H. Sato,⁹ T. Sato,⁷ M. Sekimoto,⁷ T. Shimogawa,¹ T. Shinkawa,¹² Y. Stepanenko,³ Y. Sugaya,⁸ A. Sugiyama,¹ T. Sumida,^{13,¶} Y. Tajima,⁹ S. Takita,⁹ Z. Tsamalaidze,³ T. Tsukamoto,^{1,**} Y. C. Tung,⁴ Y. W. Wah,¹¹ H. Watanabe,^{11,†} M. L. Wu,⁴ M. Yamaga,^{7,††} T. Yamanaka,⁸ H. Y. Yoshida,⁹ Y. Yoshimura,⁷ and Y. Zheng¹¹

(E391a Collaboration)

¹*Department of Physics, Saga University, Saga, 840-8502 Japan*

²*Department of Physics, Pusan National University, Busan, 609-735 Republic of Korea*

³*Laboratory of Nuclear Problems, Joint Institute for Nuclear Research, Dubna, Moscow Region, 141980 Russia*

⁴*Department of Physics, National Taiwan University, Taipei, Taiwan 10617 Republic of China*

⁵*Department of Physics and Astronomy, Arizona State University, Tempe, Arizona, USA*

⁶*Department of Particle and Nuclear Research, The Graduate University for Advanced Science (SOKENDAI), Tsukuba, Ibaraki, 305-0801 Japan*

⁷*Institute of Particle and Nuclear Studies, High Energy Accelerator Research Organization (KEK), Tsukuba, Ibaraki, 305-0801 Japan*

⁸*Department of Physics, Osaka University, Toyonaka, Osaka, 560-0043 Japan*

⁹*Department of Physics, Yamagata University, Yamagata, 990-8560 Japan*

¹⁰*Institute for High Energy Physics, Protvino, Moscow region, 142281 Russia*

¹¹*Enrico Fermi Institute, University of Chicago, Chicago, Illinois 60637, USA*

¹²*Department of Applied Physics, National Defense Academy, Yokosuka, Kanagawa, 239-8686 Japan*

¹³*Department of Physics, Kyoto University, Kyoto, 606-8502 Japan*

¹⁴*Research Center of Nuclear Physics, Osaka University, Ibaraki, Osaka, 567-0047 Japan*

(Dated: September 26, 2018)

The rare decay $K_L^0 \rightarrow \pi^0 \pi^0 \nu \bar{\nu}$ was studied with the E391a detector at the KEK 12-GeV proton synchrotron. Based on 9.4×10^9 K_L^0 decays, an upper limit of 8.1×10^{-7} was obtained for the branching fraction at 90% confidence level. We also set a limit on the $K_L^0 \rightarrow \pi^0 \pi^0 X$ ($X \rightarrow$ invisible particles) process; the limit on the branching fraction varied from 7.0×10^{-7} to 4.0×10^{-5} for the mass of X ranging from 50 MeV/ c^2 to 200 MeV/ c^2 .

I. INTRODUCTION

In the standard electroweak theory, flavor-changing neutral current (FCNC) processes are strongly suppressed and can only occur via higher-order effects. Hence, these processes will be sensitive to unknown particles or interactions that contribute in higher-order loop diagrams. Such processes are ideal places to look for signals of new physics beyond the Standard Model (SM).

In the SM, the FCNC $K_L^0 \rightarrow \pi^0 \pi^0 \nu \bar{\nu}$ decay is predominantly a CP conserving process. Its branching fraction is sensitive to the real part of the $s \rightarrow d \nu \bar{\nu}$ transition amplitude, while the related decays $K_L^0 \rightarrow \pi^0 \nu \bar{\nu}$ and $K^+ \rightarrow \pi^+ \nu \bar{\nu}$ sense the imaginary part and absolute value, respectively. Like these decays, $K_L^0 \rightarrow \pi^0 \pi^0 \nu \bar{\nu}$ is theoretically clean and uncertainties in the hadronic matrix element can be removed by using the measured branching fraction of its relevant semileptonic decay $K^+ \rightarrow \pi^0 \pi^0 e^+ \nu$.

The SM predicts the branching fraction to be $(1.4 \pm 0.4) \times 10^{-13}$ [1, 2]. Although the prediction is solid in the SM, there is a possibility of enhancements from new physics contributions. In fact, phenomenological analyses give constraints on possible enhancements by up to an order of magnitude within the allowed range of new physics parameters from known kaon decays, including the measured branching fraction of $K^+ \rightarrow \pi^+ \nu \bar{\nu}$ [2].

In addition, a new particle X which decays into invisible particles, can also contribute to the three body decay $K_L^0 \rightarrow \pi^0 \pi^0 X$. There is also a possibility of having new pseudoscalar particles, as predicted by several

* Present address: Laboratory of Nuclear Problems, Joint Institute for Nuclear Research, Dubna, Moscow Region, 141980 Russia

† Present address: Institute of Particle and Nuclear Studies, High Energy Accelerator Research Organization (KEK), Tsukuba, Ibaraki, 305-0801 Japan

‡ Present address: University of Rochester, Rochester, NY 14627

§ Present address: Scarina Gomel' State University, Gomel', BY-246699, Belarus

¶ Present address: CERN, CH-1211 Genève 23, Switzerland

** Deceased.

†† Present address: RIKEN SPring-8 Center, Sayo, Hyogo, 679-5148 Japan

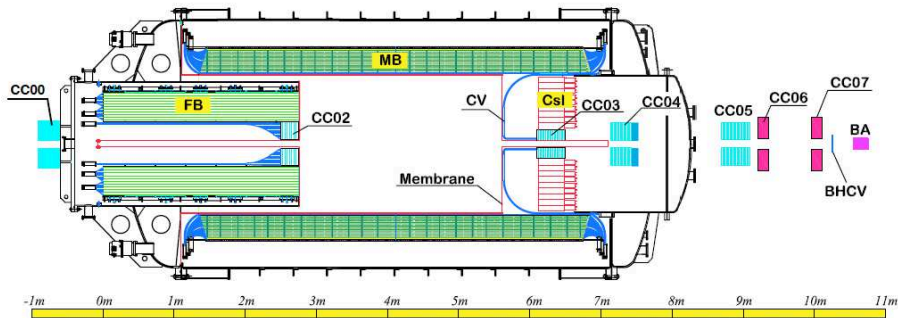


FIG. 1. Schematic cross sectional view of the E391a detector. The entrance of the detector is at “0 m.”

supersymmetry models. Searches for the $X \rightarrow \gamma\gamma$ or $X \rightarrow \mu\bar{\mu}$ modes and comparisons with the models have been made [3], and similar test should also be tried in the $\nu\bar{\nu}$ final state.

The E391a experiment at the KEK 12-GeV proton synchrotron made the first search for the $K_L^0 \rightarrow \pi^0\pi^0\nu\bar{\nu}$ decay, based on the data sample taken in the first stage (Run-I). An upper limit on the branching fraction of 4.7×10^{-5} at the 90% confidence level (C.L.) for $K_L^0 \rightarrow \pi^0\pi^0\nu\bar{\nu}$ was obtained [4]. Unfortunately the Run-I data were compromised by large neutron backgrounds from a vacuum membrane that hung in the beam. This article is based on the E391a data taken in the periods from February to April in 2005 (Run-II) and from November to December in 2005 (Run-III), after correcting the problem. These data had six times more K_L^0 decays and were analyzed with improved methods.

II. E391A DETECTOR

The E391a detector was primarily designed to search for the $K_L^0 \rightarrow \pi^0\nu\bar{\nu}$ decay [5, 6]. It had a CsI calorimeter to detect two photons from a π^0 decay and hermetic veto counters to ensure that no other visible particles existed in the final state (Fig. 1). To avoid backgrounds from interactions of the beam particles with air, most of the detector components were placed in a vacuum vessel.

The CsI calorimeter consisted of 496 blocks of $7 \times 7 \times 30$ cm³ undoped CsI crystal. A 12×12 cm² beam hole was located at the center of the calorimeter to allow the beam particles to pass through. The main barrel (MB) and front barrel (FB) counters were sandwiches of lead plates and plastic-scintillation counters with $13.5 X_0$ and $17.5 X_0$, respectively, and formed cylindrical walls surrounding the K_L^0 decay volume.

Collar shaped counters (CC00, CC02–07) were placed around the beam line for vetoing photons along the beam axis. Charged particles that would hit the CsI calorimeter were identified and rejected by energy deposits in a charge veto (CV) scintillation-counter hodoscope, located 50 cm upstream; it covered the front face as well

as the outer wall of the beam-hole area.

Beam-hole charge veto (BHCV) and back-anti (BA) counters were located in the downstream region along the beam axis and outside of the vacuum vessel. The BHCV consisted of eight 3-mm-thick plastic-scintillation counters, which were arranged to fully cover the downstream area of the beam hole. The BA was made of six superlayers, each consisting of a lead/scintillator sandwich and quartz blocks for Run-II. For Run-III the BA had five superlayers, where the lead/scintillator sandwich was replaced by the Lead Tungsten Oxide (PWO) crystals; this change was the only difference in the E391a detector system between the Run-II and Run-III periods.

Data acquisition was made with a hardware trigger that required two or more electromagnetic showers in the CsI calorimeter with total energy > 60 MeV, and no obvious activity in the CV and other veto counters. Loose on-line veto requirements were imposed, which ensured flexibility of setting energy thresholds consistently for the real data and the detector simulation during the off-line analysis. The $K_L^0 \rightarrow \pi^0\pi^0\nu\bar{\nu}$ decay should produce exactly four showers in the CsI calorimeter and nothing else in all the other counters. These hits should also satisfy an in-time requirement to suppress backgrounds.

III. DATA REDUCTION

The experimental signature of $K_L^0 \rightarrow \pi^0\pi^0\nu\bar{\nu}$ is four photons in the final states with a non-zero missing mass and a transverse momentum. Photons were registered in the CsI calorimeter as energy deposits in adjacent blocks (clusters). The most probable hit position of the photon was obtained from the shower energy distribution among the CsI blocks. Events with four photon clusters in the CsI were selected for further off-line processing.

Reconstruction of a pair of photons was made by assuming that they were from a π^0 that decayed on the beam axis (z -axis). Multiple pairings of four photons to reconstruct two π^0 s were eliminated by taking the combination that gave the minimum χ^2 value in the difference in z vertices. A cut on the minimum χ^2 for the common

z vertex V_z was effective for good π^0 identification. Also, requiring a large difference in the lowest two χ^2 values was effective in reducing the combinatorial error. We required that the common π^0 -decay vertex point V_z should be in the decay volume $300 \text{ cm} < V_z < 500 \text{ cm}$.

The veto conditions on the MB, CV, and collar counters were carefully tuned. Among these counters, the MB played a major role in vetoing photons undetected by the CsI calorimeter. If too low an energy-threshold was imposed for all of the MB counters, back-splash from the CsI/CV surface and electromagnetic shower leakage from the outer part of the CsI calorimeter to the downstream area of the MB would cause acceptance loss. Thus, we applied a tighter threshold to the upstream region of the MB to detect photons with a high efficiency, and a looser threshold to the downstream region of the MB to keep a large acceptance for the signal [7]. Suppression of the fusion cluster (misidentification of two close-by clusters as one cluster) was made by using the neural network (NN) technique trained by the stand-alone photons and the fusion clusters from the $K_L^0 \rightarrow \pi^0\pi^0\pi^0$ Monte Carlo (MC) simulation sample. Further suppression was made on the shower shape of the cluster, and by examining the energy distribution and its RMS fraction [7].

TABLE I. Reduction factors and resultant acceptances in each data reduction step (signal Monte Carlo).

Cuts	Reduction factor	Resultant acceptance
K_L^0 decay in the fiducial volume		1.00
+ hardware trigger & four-cluster-candidate in the CsI calorimeter	0.0499	4.99×10^{-2}
+ tighter CsI fiducial	0.616	3.08×10^{-2}
+ rejection of fused cluster	0.361	1.11×10^{-2}
+ req. good cluster	0.295	3.28×10^{-3}
+ χ^2 cut for two π^0 vertex matching	0.606	1.99×10^{-3}
+ other misc. requirements on CsI	0.829	1.65×10^{-3}
+ MB and upstream Vetoes	0.621	1.02×10^{-3}
+ downstream Vetoes	0.853	8.74×10^{-4}
+ req. signal box (after all the cuts)	0.346	3.02×10^{-4}

IV. MC SIMULATION

A GEANT3-based [8] MC simulation was performed to define the signal region for $K_L^0 \rightarrow \pi^0\pi^0\nu\bar{\nu}$ and to estimate the acceptance. The $K_L^0 \rightarrow \pi^0\pi^0\nu\bar{\nu}$ decay was generated with the V-A interaction, and the events were processed with the same reconstruction code as the real data. Among the incoming K_L^0 particles to the detector, 2.66% decay within the fiducial decay volume. A total of 1×10^8 incoming K_L^0 events were generated for both Run-II and Run-III. The generated events were overlaid with accidental hits on the counters accumulated by special triggers during the data taking. After applying the selection criteria described above, a two-dimensional distribution of the $\pi^0\pi^0$ effective mass $M_{\pi^0\pi^0}$ and the transverse momentum P_T for the accepted events was examined. The result of the simulation for $K_L^0 \rightarrow \pi^0\pi^0\nu\bar{\nu}$ in the Run-III condition is shown in Fig. 2(a).

The signal region was defined as a right triangular area shown in Fig. 2. The vertical edge of the triangle is located at the lower bound of the $\pi^0\pi^0$ effective mass (0.268 GeV/c^2), and spanned the P_T values between 0.1 to 0.2 GeV/c . The horizontal edge defined the lower bound of P_T (0.1 GeV/c) to avoid contamination from the $K_L^0 \rightarrow \pi^0\pi^0\pi^0$ decay; it spanned the $M_{\pi^0\pi^0}$ values between 0.268 to 0.450 GeV/c^2 .

The detector acceptance was calculated by taking the ratio of the number of events in the signal region to the number of K_L^0 particles that decayed in the fiducial vertex region. A list of the reduction factors that contributed to the acceptance after the K_L^0 s decayed in the fiducial volume are summarized in Table I. The acceptances obtained for Run-II and Run-III were consistent, and the result was $(3.02 \pm 0.11_{stat.}) \times 10^{-4}$ for each run period.

To study the dominant backgrounds, MC events of the $K_L^0 \rightarrow \pi^0\pi^0$ decay with the statistics equivalent to 11.2 and 11.9 times the Run-II and Run-III data, and the $K_L^0 \rightarrow \pi^0\pi^0\pi^0$ decay equivalent to 0.80 and 2.52 times the Run-II and Run-III data, respectively, were generated with the same detector conditions as the real data.

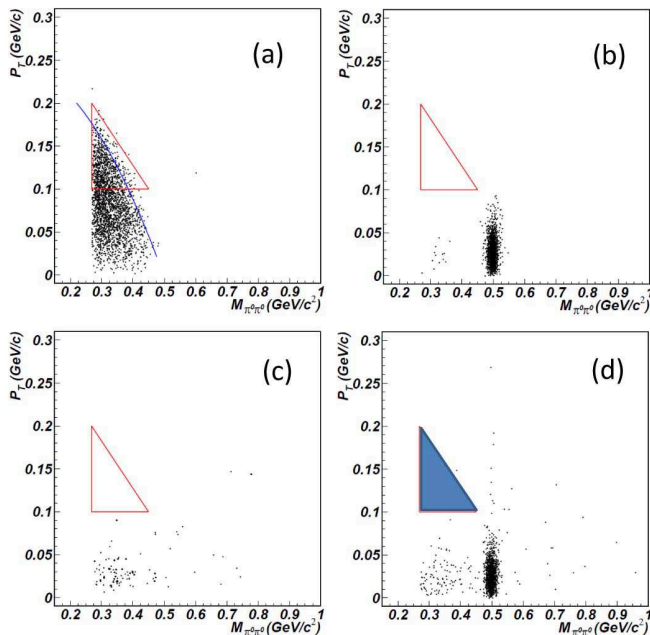


FIG. 2. P_T vs. effective mass ($M_{\pi^0\pi^0}$) plots of the $\pi^0\pi^0$ system from Run-III MC simulations for (a) $K_L^0 \rightarrow \pi^0\pi^0\nu\bar{\nu}$, (b) $K_L^0 \rightarrow \pi^0\pi^0$, (c) $K_L^0 \rightarrow \pi^0\pi^0\pi^0$, and (d) Run-III real data. The statistics of the MC events in (b) and (c) are normalized to those of the real data. The signal region is defined to be inside of the triangular area in the plots. A curved line in (a) indicates the kinematical limit for the $K_L^0 \rightarrow \pi^0\pi^0\nu\bar{\nu}$ decay.

Within these statistics, no MC events of these processes were found in the $K_L^0 \rightarrow \pi^0 \pi^0 \nu \bar{\nu}$ signal region for both the Run-II and Run-III conditions.

The MC results of the $K_L^0 \rightarrow \pi^0 \pi^0$ and $K_L^0 \rightarrow \pi^0 \pi^0 \pi^0$ decays for the Run-III condition, with the same statistics as the real data, are shown in Figs. 2(b) and (c), respectively, together with the Run-III real data (Fig. 2(d)). The $K_L^0 \rightarrow \pi^0 \pi^0$ plot of P_T vs. $M_{\pi^0 \pi^0}$ showed clear clustering well removed from the signal region of $K_L^0 \rightarrow \pi^0 \pi^0 \nu \bar{\nu}$ (Fig. 2(b)). Events from the $K_L^0 \rightarrow \pi^0 \pi^0 \pi^0$ decay were spread over the P_T vs. $M_{\pi^0 \pi^0}$ plot without having clear boundaries (Fig. 2(c)). The data plot (Fig. 2(d)) outside of the masked signal region was characterized by the sum of Fig. 2(b) and (c), except for a small number of events that extended to higher P_T from the $K_L^0 \rightarrow \pi^0 \pi^0$ cluster region. These latter events are considered to be due to K_S^0 regeneration in the detector, and are not simulated in the MC. They will be discussed in Sec. VI. The MC study showed that most events stayed close to the signal region except that those for $M_{\pi^0 \pi^0} \approx M_{K^0}$ were from $K_L^0 \rightarrow \pi^0 \pi^0$ and $K_L^0 \rightarrow \pi^0 \pi^0 \pi^0$ decays. The main background source was $K_L^0 \rightarrow \pi^0 \pi^0 \pi^0$.

V. SENSITIVITY

The number of K_L^0 particles that decayed in the fiducial vertex region was estimated by detecting $K_L^0 \rightarrow \pi^0 \pi^0$ with the same π^0 selection criteria in the CsI calorimeter as for $K_L^0 \rightarrow \pi^0 \pi^0 \nu \bar{\nu}$. Comparison with the MC simulation of $K_L^0 \rightarrow \pi^0 \pi^0$, with the same π^0 selection criteria as the real data, along with overlaid accidental events, gave the number of K_L^0 decays as $(5.48 \pm 0.09_{stat.} \pm 0.31_{sys.}) \times 10^9$ for Run-II and $(3.88 \pm 0.08_{stat.} \pm 0.21_{sys.}) \times 10^9$ for Run-III, respectively.

To estimate the systematic uncertainties, the fractional difference between the data and the MC simulation in each selection criteria was examined, and the quadratic sum weighted by the effectiveness of each of the acceptance determinations [6] was taken. The calculated values were 5.6% and 5.5% for Run-II and Run-III, respectively. The same values of the systematic uncertainty were adopted to the $K_L^0 \rightarrow \pi^0 \pi^0 \nu \bar{\nu}$ decay.

Based on the acceptance for the $K_L^0 \rightarrow \pi^0 \pi^0 \nu \bar{\nu}$ decay obtained from the MC simulation, and the number of K_L^0 decays in the data-taking runs, the single event sensitivity (S.E.S) was defined as

$$S.E.S. = \frac{1}{\text{Acceptance} \times \text{Number of } K_L^0 \text{ decays}}.$$

The S.E.S. was derived as $(6.04 \pm 0.24_{stat.} \pm 0.48_{sys.}) \times 10^{-7}$ for Run-II and $(8.53 \pm 0.35_{stat.} \pm 0.66_{sys.}) \times 10^{-7}$ for Run-III. The combined S.E.S. was $(3.54 \pm 0.10_{stat.} \pm 0.28_{sys.}) \times 10^{-7}$. The sensitivity reported here is considerably improved from that of our previous analysis [4]. In addition to the six-times larger statistics, the acceptance factor was improved for several selection criteria. Examples include the adoption of a looser cut for χ^2 in

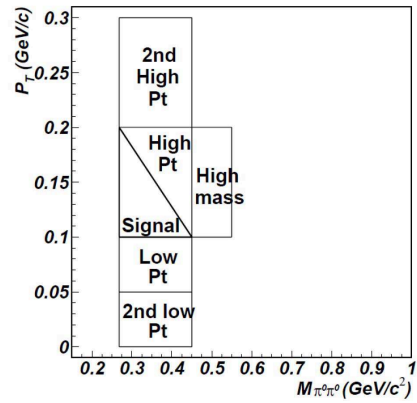


FIG. 3. Kinematic boundaries of P_T vs. $M_{\pi^0 \pi^0}$ for the bifurcation analysis.

TABLE II. Numbers of the events in the real data (Run-II and Run-III combined) selected by the combinations of two cut sets, A and B, at various regions defined in Fig. 3. They were used for the estimations of N_{bkg} in the bifurcation method. N_{AB} is the observed number of events in those regions.

Region	$N_{A\bar{B}}$	$N_{\bar{A}B}$	$N_{\bar{A}\bar{B}}$	Est. N_{bkg}	N_{AB}
Signal	3	381	2508	0.46 ± 0.26	–
Low P_T	136	6330	41418	20.8 ± 1.8	21
2nd low P_T	1151	17525	105455	191.3 ± 5.9	229
High P_T	0	110	604	0.0	1
2nd high P_T	1	5	41	0.12 ± 0.13	0
High Mass	6	283	1086	1.56 ± 0.65	12

the two- π^0 vertex matching, and optimizing the criteria used to select good photon clusters in the CsI calorimeter, both of which were possible in a cleaner environment with less neutron background in Run-II and Run-III.

VI. BACKGROUND ESTIMATION

A “blind analysis” technique was used to minimize the contribution from backgrounds without examining the candidate events in the signal region. Among the background sources, $K_L^0 \rightarrow \pi^0 \pi^0$ was fully reconstructed and rejected primarily by kinematic variables (P_T , $M_{\pi^0 \pi^0}$) of the $\pi^0 \pi^0$ system. However, $K_L^0 \rightarrow \pi^0 \pi^0 \pi^0$ would become a background if two photons were missed due to finite photon-veto inefficiencies in the detector. The kinematic cuts could not be applicable to this dominant background source, and suppression depended strongly on the photon veto conditions.

To avoid the difficulty of having enough statistics in the MC simulation of the $K_L^0 \rightarrow \pi^0 \pi^0 \pi^0$ background in the signal region, we adopted the “bifurcation method” to estimate the number of background events in the signal region from the real data [4, 9]. We imposed several selection criteria (cuts) to identify the $K_L^0 \rightarrow \pi^0 \pi^0 \nu \bar{\nu}$ signal from backgrounds, and the roles of these cuts were

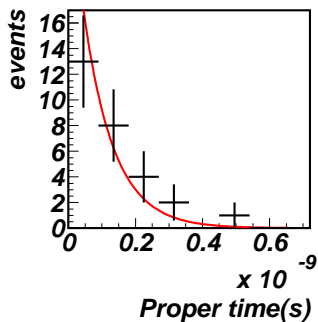


FIG. 4. Proper-time distribution of the $\pi^0\pi^0$ system for the events with $P_T \geq 0.1$ GeV/c and $0.45 \leq M_{\pi^0\pi^0} \leq 0.55$ GeV/c² with a loose requirement for V_z for the Run-II and Run-III, assuming the production point was on the downstream edge of CC02. The solid line is an expectation from the $K_S^0 \rightarrow \pi^0\pi^0$ decay.

categorized in two groups, namely cut A and cut B . The cut A consisted of “veto” requirements to ensure no particles other than from the CsI-calorimeter region, and the cut B consisted of the cuts to select well-reconstructed π^0 s from pairs of photon clusters in the calorimeter.

If the two categories of cuts are uncorrelated, the number of events that passed both of the cuts A and B would be described as

$$N_{AB} \equiv N_0 P(AB) \cong N_0 P(A)P(B),$$

where N_0 is the number of events after the basic “setup cuts” are imposed prior to the cuts A and B , and $P(A)$, $P(B)$ and $P(AB)$ are the probability of passing the conditions A , B , and AB , respectively. The number of estimated background events N_{bkg} is derived as

$$\begin{aligned} N_{bkg} &= N_0 P(A)P(B) \\ &= \frac{N_0 P(A)P(\bar{B})N_0 P(\bar{A})P(B)}{N_0 P(\bar{A})P(\bar{B})} \\ &= \frac{N_0 P(A\bar{B})N_0 P(\bar{A}B)}{N_0 P(\bar{A}\bar{B})} = \frac{N_{A\bar{B}}N_{\bar{A}B}}{N_{\bar{A}\bar{B}}}, \end{aligned}$$

where the symbols \bar{A} and \bar{B} are the inverse logic of A and B , respectively. Thus N_{bkg} in the signal region after imposing all of the cuts A and B could be estimated from the number of events obtained by the combination of $A\bar{B}$, $\bar{A}B$, and $\bar{A}\bar{B}$.

The kinematic region defined by P_T and $M_{\pi^0\pi^0}$ of the $\pi^0\pi^0$ system was further divided into six as shown in Fig. 3. For each region, N_{bkg} was estimated by the formula above.

Table II summarizes the background estimates for the Run-II and Run-III data combined. Various kinematic regions were tabulated to cross-check the validity of this method. The numbers of events of the real data N_{AB} are consistent with the estimated values N_{bkg} , and also agree reasonably with the MC results of dominant backgrounds (sum of $K_L^0 \rightarrow \pi^0\pi^0$ and $\pi^0\pi^0\pi^0$ decays), after

TABLE III. Comparison of MC events of background processes ($K_L^0 \rightarrow \pi^0\pi^0$ and $K_L^0 \rightarrow \pi^0\pi^0\pi^0$) after imposing cuts A and B and real data in the kinematic regions given in table II. The MC results are normalized to the K_L^0 flux for the real data.

Region	$K_L^0 \rightarrow \pi^0\pi^0$ (MC)	$K_L^0 \rightarrow \pi^0\pi^0\pi^0$ (MC)	Sum of the two MC	Real data
Signal	0.0	0.0	0.0	—
Low P_T	0.5	15.6	16.1	21
2nd low P_T	11.9	203.1	215.0	229
High P_T	0.1	0.0	0.1	1
2nd high P_T	0.0	0.0	0.0	0
High Mass	0.2	0.0	0.2	12

imposing the cuts A and B (Table III) in most of the regions around the signal region.

The real data (12 events) in the “High mass” region exceeded the estimated number of events (1.56 ± 0.65 events). These events are seen in Fig. 2(d) with $M_{\pi^0\pi^0}$ around M_{K^0} , extending to the higher P_T region (≥ 0.1 GeV/c). Fig. 4 shows the proper-time distribution of the $\pi^0\pi^0$ system with $P_T \geq 0.1$ GeV/c, $0.45 \leq M_{\pi^0\pi^0} \leq 0.55$ GeV/c², and a looser V_z requirement for the Run-II and Run-III combined, assuming that the production point was the downstream edge of the CC02 counter. The proper-time distribution (Fig. 4) is consistent with that of expected from the $K_S^0 \rightarrow \pi^0\pi^0$ decay, implying that the events are from regeneration of K_S^0 in the upstream materials and subsequent $\pi^0\pi^0$ decay.

Because the final state of the $K_S^0 \rightarrow \pi^0\pi^0$ process was fully reconstructed, these events were insensitive to the photon-veto cuts (cuts A) and also to the CsI cluster shape cuts (cuts B). Hence the bifurcation method was not applicable for estimating the backgrounds from this process. Nevertheless, these events might occur in the signal region by a mis-pairing of the photons from the π^0 s. Assuming that the mis-pairing rate for $K_S^0 \rightarrow \pi^0\pi^0$ decays was equal to that for $K_L^0 \rightarrow \pi^0\pi^0$ decays shown in Fig. 2(b), the contribution of events in the “High mass” region to the signal region was negligibly small (< 0.03 events).

The number of background events in the signal region was estimated to be 0.46 ± 0.26 for the Run-II and Run-III combined (Table II).

In the discussions above, we assumed that the cut sets A and B were uncorrelated. A measure of the correlation was given by the parameter $\epsilon \equiv P(A|B) - P(A|\bar{B})$, as the difference of the probability of satisfying the cut A for the events that passed the cut B , and for the events that passed the cut \bar{B} . Corrections to the N_{bkg} due to the correlation are given by

$$C_\epsilon = \epsilon \times N_{\bar{A}\bar{B}} \left(1 + \frac{N_{bkg}}{N_{\bar{A}\bar{B}}} \right)$$

to first order of ϵ [4, 10]. In the “Low P_T ” region, which was closest to the signal region, ϵ was $(0.34 \pm 7.73) \times 10^{-4}$.

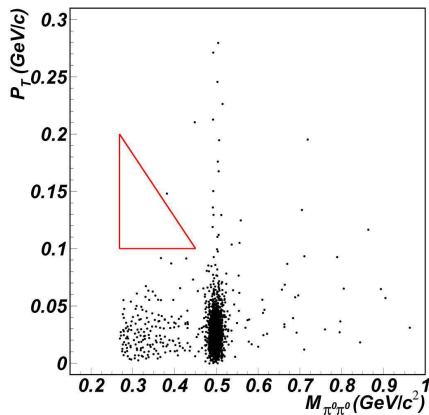


FIG. 5. P_T vs. $M_{\pi^0\pi^0}$ distribution for Run-II and Run-III combined.

TABLE IV. Summary of the acceptance, S.E.S., and 90% C.L. upper limit on the branching fraction with several assumptions of the mass of X in the $K_L^0 \rightarrow \pi^0\pi^0 X$ ($X \rightarrow$ invisible particles) decay.

M_X (MeV/ c^2)	accep- tance	S.E.S.	Br upper limit with 90% C.L.
50	3.52×10^{-4}	3.04×10^{-7}	7.0×10^{-7}
75	3.50×10^{-4}	3.05×10^{-7}	7.0×10^{-7}
100	3.45×10^{-4}	3.10×10^{-7}	7.1×10^{-7}
125	2.91×10^{-4}	3.67×10^{-7}	8.5×10^{-7}
150	2.07×10^{-4}	5.16×10^{-7}	1.2×10^{-6}
175	9.18×10^{-5}	1.16×10^{-6}	2.7×10^{-6}
200	6.21×10^{-6}	1.72×10^{-5}	4.0×10^{-5}

Applying this value to the signal region, the correction to be made to the N_{bkg} was 0.01 ± 0.29 events. The magnitude of the correction is small compared with the quoted error for the N_{bkg} , and this effect was not taken into account in deriving the final result.

VII. RESULTS

After all of these studies, the candidate events in the signal region were examined. Figure 5 shows the com-

bined results of the Run-II and Run-III; no events are observed in the signal region. By using Poisson statistics with zero background events in the signal region, we set an upper limit on the branching fraction of $K_L^0 \rightarrow \pi^0\pi^0\nu\bar{\nu}$ to be 8.1×10^{-7} at the 90% C.L. The systematic uncertainty in the S.E.S. is not taken into account in the limit.

From the same data sample, we also derived the upper limit on the $K_L^0 \rightarrow \pi^0\pi^0 X$ ($X \rightarrow$ invisible particles) decay assuming three-body phase space. Because the acceptance depended on the mass of X , the upper limit was obtained as a function of the assumed mass of X as summarized in Table IV.

There are prospects of further improving the limit. A new experiment E14 is now in preparation at J-PARC [11], aiming at studying the $K_L^0 \rightarrow \pi^0\nu\bar{\nu}$ decay with three orders-of-magnitude higher sensitivity than E391a by utilizing higher beam flux, longer beam time, and an upgraded detector with CsI calorimeter of higher efficiency and granularity. Further increases of the beam flux are planned in the upgrade. In the case of $K_L^0 \rightarrow \pi^0\pi^0\nu\bar{\nu}$, improving the photon cluster detection in the CsI calorimeter is essential to improving the sensitivity. Hence we are hopeful to have significant progress on this process in the near future.

ACKNOWLEDGMENTS

We are grateful to the operating crew of the KEK 12-GeV proton synchrotron for the successful beam operation during the experiment. This work has been partly supported by a Grant-in-Aid from the MEXT and JSPS in Japan, a grant from NSC and Ministry of Education in Taiwan, from the U.S. Department of Energy and from the Korea Research Foundation.

-
- [1] L.S. Littenberg and G. Valencia, Phys. Lett. **B385**, 379 (1996).
 - [2] C.W. Chiang and F.J. Gilman, Phys. Rev. **D62**, 094026 (2000).
 - [3] Y.C. Tung *et al.*, Phys. Rev. Lett. **102**, 051802 (2009); H.J. Hyun *et al.*, Phys. Rev. Lett. **105**, 0091801 (2010); E. Abouzaid *et al.*, e-print: arXiv:1105.4800[hep-ex].
 - [4] J. Nix *et al.*, Phys. Rev. **D76**, 011101(R) (2007).
 - [5] J.K. Ahn *et al.*, Phys. Rev. **D74**, 051105(R) (2006) ; Phys. Rev. Lett. **100**, 201802 (2008).
 - [6] J.K. Ahn *et al.*, Phys. Rev. **D81**, 072004 (2010).
 - [7] Y.C. Tung *et al.*, Phys. Rev. **D83**, 031101(R) (2010).
 - [8] R. Brun, F. Bruyant, M. Maire, A.C. McPherson, P. Zanarini, CERN-DD-EE-84-1, Sep 1987. Revised version.
 - [9] S. Adler *et al.*, Phys. Rev. Lett. **79**, 2204 (1997), Phys. Rev. **D77**, 052003 (2008).
 - [10] J. Nix *et al.*, Nucl. Instr. and Methods **A615**, 223 (2010).
 - [11] J. Comfort *et al.*, (J-PARC E14 Collaboration), "Proposal for $K_L^0 \rightarrow \pi^0\nu\bar{\nu}$ Experiment at J-Parc" (2006).